Statics and dynamics of model dendrimers as studied by molecular dynamics simulations

K. Karatasos,[a] D. B. Adolf, and G. R. Davies
Department of Physics and Astronomy, University of Leeds, Leeds LS2 9JT, United Kingdom

(Received 15 May 2001; accepted 22 June 2001)

Molecular dynamics simulations were performed for a series of AB_2 dendrimer models, in explicit-solvent solutions where the ratio R_g/L (R_g is the radius of gyration and L the size of the simulation box) is kept between $0.15 \leqslant R_g/L \leqslant 0.2$. Results on static properties (size, shape, density profiles) are in good agreement with recent theoretical and experimental studies. Dynamic properties are systematically investigated on the local and entire molecule length scale. The dynamic characteristics of the examined models capture the qualitative behavior observed experimentally in dendrimer molecules. The systematic and comparative nature of this study affords detailed insight into the origin and the relative contribution of different relaxational mechanisms in the observed dynamic spectra. © *2001 American Institute of Physics.* [DOI: 10.1063/1.1394207]

I. INTRODUCTION

Dendrimers have been a subject of growing interest in the past two decades motivated by the large number of potential applications for these novel molecules.[1,2] Biological applications such as molecular recognition[3,4] or delivery vehicles for bioreactive molecules[1,5] take advantage of the unique molecular architecture of these materials while their use as polymer rheology modifiers or processing aids[6,7] exploit their transport/dynamic properties.[8–11] Ever growing and maturing chemistry protocols are allowing for property-driven syntheses[3,12] affording well characterized molecules with low polydispersity and a minimal number of defects in the target morphology.[2,13] The availability of these materials fosters new research into the structure-property relationships of these highly branched materials. Comparatively speaking, most of these efforts concentrate on static quantities relative to dynamic quantities affording large gaps in our understanding of these materials.[14–29] With this in mind, the aim of this work is to explore the interrelation between the spatial size and the structural/dynamic properties of dendrimer molecules and to proceed in a qualitative comparison to experimental findings. Special emphasis is placed on investigating the relaxational characteristics of the examined models.

The paper is organized as follows: In Sec. II details are given concerning the topology of the dendritic models used and the relevant simulation parameters. Key static/structural properties of the examined systems are described in Sec. III and are compared to available theoretical and experimental findings of dendrimer molecules. In Sec. IV a detailed analysis of the dynamic characteristics of dendrimers is performed to study relaxational mechanisms spanning a range of length scales from a bond length up to the size of the entire dendrimer. Section V summarizes the main findings and discusses the general picture emerging from this study.

[a]Author to whom all correspondence should be addressed; electronic mail: kkaratas@ulb.ac.be

II. SIMULATION DETAILS

A. Description of the models

AB_2 dendrimers of generations (G) 3, 4, 5, and 6 were simulated in solution in the presence of explicit solvent molecules, at a volume fraction of approximately 4%. This ensured that the ratio of the dendrimers' size (as expressed by the radius of gyration R_g) over the simulation box size L, was kept as low as $0.15 \leqslant R_g/L \leqslant 0.20$. The total number of atoms in the simulation box amounted to $N_{G=3}=2049$, $N_{G=4}=4122$, $N_{G=5}=8711$, and $N_{G=6}=16\,425$.

As the intention was to investigate generic properties arising from dendrimer topology, a freely joined bead–spring model, commonly employed in theoretical studies, was adopted. The dendrimer beads were represented as united atoms (UAs) with mass corresponding to a CH_i group, where i is determined by the connectivity of each bead (e.g., $i=3$ if a bead is connected to only one other bead). Each solvent molecule was represented by a UA CH_4 group.

The model chosen should be placed in the general category of coarse-grained models which have frequently been employed in theoretical[30–32] or computational studies[11,19,20,33] in order to study basic characteristic features of dendrimer molecules. In previous computational efforts of such dendrimer models, solution systems were studied by Molecular Dynamics (MD) employing uncorrelated white noise,[20] or with Brownian dynamics techniques invoking correlations/hydrodynamic interactions (HIs) through the use of the Rotne–Prager–Yamakawa tensor.[11] On these grounds, our model where the solvent is explicitly represented by discrete molecules is a step forward since HIs are implicitly introduced through the correlations between the solvent and the dendrimer beads with no other *a priori* assumptions. Nevertheless, it must be pointed out that a systematic investigation of finite size effects on the static and, most importantly, on the dynamic properties of the examined models is beyond the scope of the present work. Since, to our knowl-

edge, such a systematic study has not yet been performed for dendrimer molecules, our approach for the treatment of periodic boundary conditions/finite size effects is based on previous simulations of linear polymers in explicit-solvent solutions. The authors of Ref. 34 studied the finite size effects in transport and dynamic properties of single freely joined chains of varying length, at high dilution conditions where $0.1<R_g/L<0.3$. It was found that in this range the static properties of the chains did not present box-size effects, whereas the intermediate scattering function $S(q,t)$ (q is the scattering vector) appeared to be box-size dependent at the low q regime. This effect was attributed to the increase of the center of mass diffusion with the box size and found to be adequately described with the aid of the Kirkwood formula for the chain diffusion coefficient after suitable modification[35] to incorporate image chain effects. This treatment, which was further discussed in Ref. 36, showed that apart from a numerical prefactor, the diffusion coefficient of the chain was a universal function of the ratio R_g/L. This ratio in the systems of Ref. 36 amounted to 0.195, 0.225, and 0.228. Furthermore, regarding the dynamic behavior, it was shown[34] that despite the q dependence of $S(q,t)$ on the box size (weak for high q and more significant for lower q values), the local reorientational dynamics as described by the bond autocorrelation function yielded indistinguishable results for different box sizes (see Fig. 3 of Ref. 34). Moreover, this insensitivity to the box size was also observed in the behavior of correlation functions related to global chain dimensions[37] like the square end-to-end distance and the end-to-end vector autocorrelation functions.

Occurrence of the same behavior in a representative of our dendrimer models ($G=3$) was confirmed by studying local and global reorientational dynamics after reducing the volume fraction (by increasing the box size and more than doubling the number of solvent molecules) to 1.8%. Differences between the 4% and the 1.8% systems in the calculated autocorrelation functions related to the length scale of a single bond or that of the entire dendrimer size were well within the error bars. Analogously, it is assumed that reorientational dynamics of the other dendrimer systems, follow the same degree of insensitivity to box-size effects. It must also be noted that even without this direct analogy the low and approximately constant R_g/L ratio for our systems should be sufficient to validate any *relative* comparison between the different dendrimer molecules examined.

The dendrimer topology invoked is schematically illustrated in Fig. 1. The structure emerges from a trifunctional core and emanates radially outward with bifunctional branching of every other bead. According to this scheme, a dendrimer grown to the Gth generation ($G=0,1,...$) consists of $N_G=3P(2^{G+1}-1)+1$ beads. P is the number of bonds between branching points and is 2 in this case. The total number of generations for a given dendrimer model is denoted by G while g will refer to beads belonging to the gth shell of the dendrimer. A $G=0$ dendrimer contains the core with three bonds each connecting it to a pair of bonded UA.

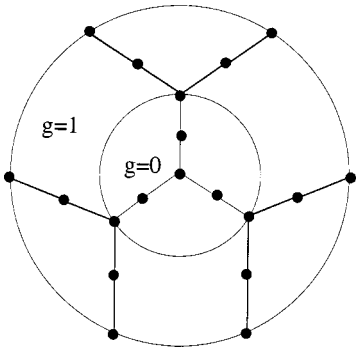

FIG. 1. Schematical representation of the dendrimer models examined.

B. Simulation parameters

The bonds between the beads are allowed to fluctuate harmonically around an equilibrium value with a potential energy as described by $U_{\text{bond}}=\frac{1}{2}k(l-l_0)^2$. The parameters $k=158.35$ kcal/mol and $l_0=1.54$ Å used are typical for the description of linear hydrocarbon polymers.[38] A Lennard-Jones potential $U(r_{ij})=4\epsilon[(\sigma/r_{ij})^{12}-(\sigma/r_{ij})^6]$ is employed for the calculation of the nonbonded interactions between any pair of united atoms (i.e., dendrimer and solvent). A cutoff of $r_{\text{cut}}=2.5\sigma$ is used and the σ parameter is set equal to l_0 allowing simulations to be performed within the limit of high excluded volume. Dendrimer beads and solvent beads are assigned the same σ value. The energetic parameter ϵ was 0.113 kcal/mol and the simulation temperature was chosen so that $\epsilon=0.3k_BT$, following Rey *et al.*,[39] where it is shown to reproduce Θ condition of linear polymers. Since definition of an "exact" Θ condition for a dendrimer molecule is not a simple task due to the nature of the many-body interactions involved,[40] the temperature corresponding to the Θ condition in linear chains was examined, in order to facilitate comparison to previous theoretical[30] and computational[20] studies of similar dendrimer models, where results corresponding to this condition are available.

The simulations were performed within the DL_POLY molecular dynamics package.[41] The time step used was 1 fs corresponding to $\Delta t=0.0012\tau$, where $\tau=\sigma(m/\epsilon)^{1/2}$ is the characteristic time of the model (m is the average mass per bead, 13.7 amu). From now on, l_0 and τ will be used as the standard units for length and time, respectively. Each system is equilibrated for about 2×10^6 time steps in the NVT ensemble after which the mean square radius of gyration ($\langle R_g^2\rangle$) reached equilibrium. Production runs are then performed for at least 10^7 time steps in the NVE ensemble.

III. STATIC/STRUCTURAL PROPERTIES

Figure 2 shows R_g^2 for $G=3$ through $G=6$ dendrimers as a function of time during the production run. The average size of the dendrimer remains stable during the entire trajectory. Table I lists the values of $\langle R_g^2\rangle$ with the corresponding standard deviations as a function of generation number and total number of beads per dendrimer molecule (N). The dependence of R_g on the total number of beads per dendrimer N follows the power law $R_g\propto N^x$ where $x=0.35\pm0.03$. The

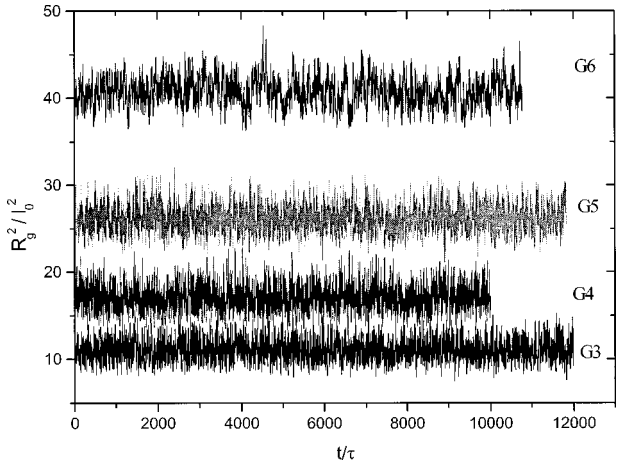

FIG. 2. Instantaneous values of the R_g^2.

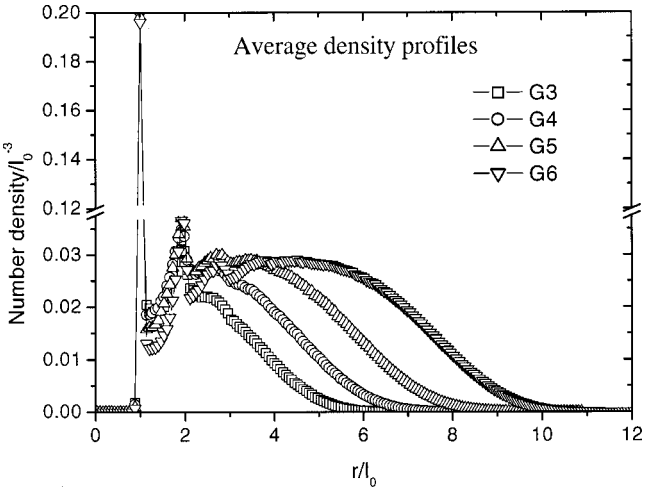

FIG. 3. Average bead number densities of the examined models. The peaks observed at distances $r=l_0$ and $r\simeq 2l_0$ correspond to one and two bond lengths of the 0th generation beads.

calculated exponent is in a very good agreement with the exponent $x=1/3$ which was predicted by numerical calculations[18] (see Figs. 5 and 6 where results from the method discussed are compared to results from simulations) and observed in several simulations[20,28,33] and experimental[14,23,25] studies of dendrimer systems.

Such a scaling behavior is characteristic[20] of three-dimensional compact objects being consistent with the results from structural studies of flexible dendrimer molecules in solution.[42] The implied space filling geometry requires a considerable degree of backfolding of the outer generation beads. Although this conjecture is in disagreement with early theoretical efforts,[43] its validity is illustrated in previous numerical calculations and computer simulations[18,20,25,44] and verified by recent experimental studies of dendrimer molecules.[23,27,45,46] Specifically, the extent of inward folding increases with the dendrimer G value. The results reported here are in accord with these findings. Figure 3 shows the average number densities of dendrimer beads as a function of the distance from the core for the $G3-G6$ molecules. The density profiles exhibit a plateau which broadens with increasing G value followed by a monotonic decrease toward the exterior of the molecule. It is of interest to resolve the spatial distribution of beads belonging to topologically different generation shells (i.e., each g value) within these profiles. Figure 4 illustrates the number density profiles due to the successive generation shells in the $G6$ dendrimer. Evidently, the degree of backfolding increases with the generation shell. The beads of the outer shell ($g=6$) are found throughout the dendrimer including distances close to the trifunctional core. The inset of Fig. 4 shows the corresponding histograms of radial distances of the beads from the center, with the location of the peak representing the average (solid line) signifying the R_g of the molecule. The peaks corresponding to different generational shells are shifted to longer distances as g increases, and the tails of the distributions extend close to the center. Solid-state REDOR nuclear magnetic resonance (NMR) measurements on flexible dendrons revealed close contact between the focal and peripheral groups.[45] In addition, longitudinal NMR relaxation times in paramagnetic core dendrimers indicated a close approach of all units within a dendrimer to the molecular core.[47]

Insight into the actual shape of the simulated dendrimers as a function of the generation number, G, can be extracted from calculation of the molecular form factors and the relative aspect ratios along the principal axis of inertia. In Fig. 5, the scattering functions of the examined dendrimers are shown in the Kratky representation. The solid line denotes the form factor of a compact sphere with radius of gyration the same as that of the $G6$ dendrimer. Besides the major peak at $qR_g\simeq 1.7$, a secondary peak is clearly resolved, es-

TABLE I. Mean squared radius of gyration of the simulated systems.

G	N	$\langle R_g^2\rangle/l_0^2$	Standard deviation
3	91	11.06	1.17
4	187	17.13	1.41
5	379	26.12	1.47
6	673	40.86	1.53

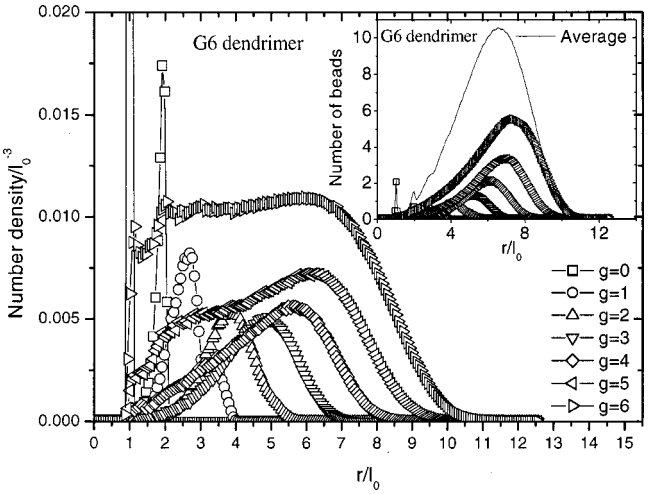

FIG. 4. $G6$ model: bead number densities resolved in generational shells. Inset: the corresponding histogram of the number of beads as a function of the radial distance from the core.

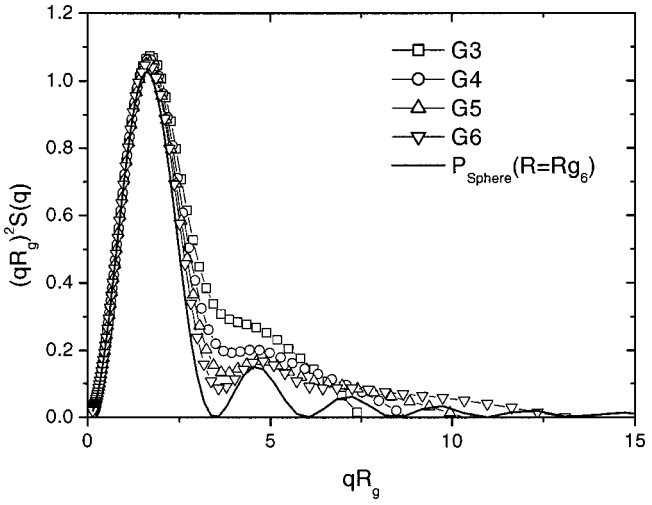

FIG. 5. Kratky plots for the studied dendrimer models. The solid line corresponds to a solid sphere with radius equal to the radius of gyration of the $G6$ model.

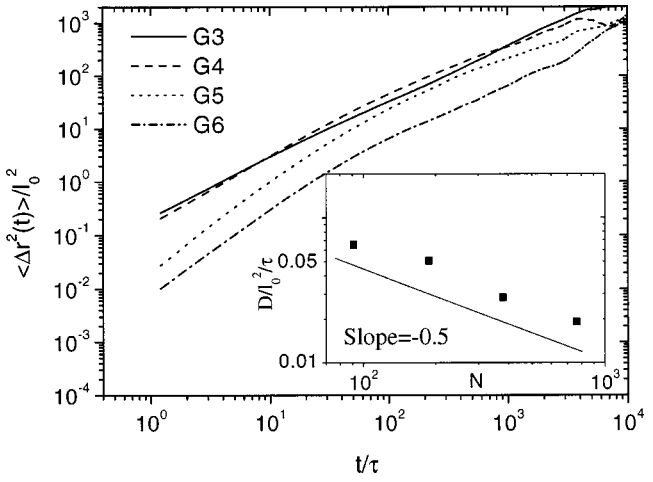

FIG. 7. Mean square displacement of the center of mass of the examined dendrimer models. The inset depicts the diffusion coefficient as a function of beads per dendrimer.

pecially for the higher generation models at $qR_g \simeq 4.8$ in accordance with the location of the second-order peak of the hard spherical geometry. The appearance of higher order peaks in dendrimer scattering functions has been reported in other numerical[18] and computational[48] studies of dendrimer models. Experimentally, x-ray scattering data from high generation dendrimers exhibited a two side maxima in the measured small-angle scattering intensity as a function of the magnitude of the scattering vector, while observation of a secondary peak in the range of $qR_g \simeq 4-5$ has recently been reported in small-angle neutron scattering experiments[25,49] of high generation poly(propyleneimine) and poly(amidoamine) (PAMAM) dendrimers.

Supplemental information pertinent to the geometry of the simulated models is obtained by examining the moment of inertia of the systems. The aspect ratios I_z/I_x and I_z/I_y where I_z, I_y, I_x represent the eigenvalues of the moment of inertia tensor in descending order, are plotted in Fig. 6. Low generation dendrimers are asymmetric, while higher generations assume a more globular structure as denoted from the progressive decrease of the aspect ratios toward unity.

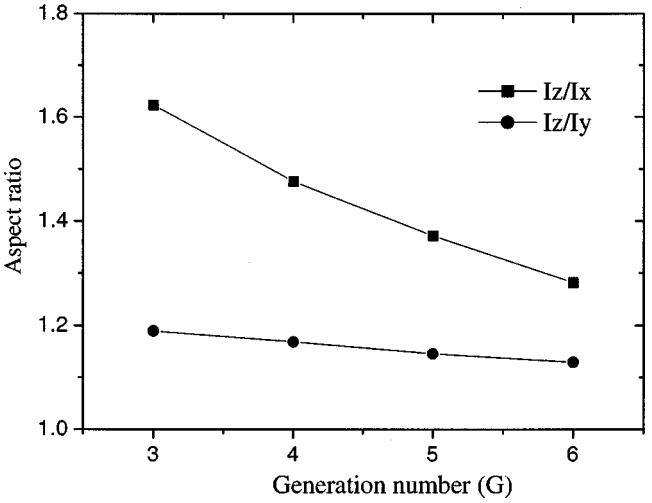

FIG. 6. Moment of inertia aspect ratios as a function of generation number, where $I_z \geqslant I_y \geqslant I_x$.

IV. DYNAMIC/TRANSPORT PROPERTIES

The G value of a dendrimer heavily influences its dynamic behavior[31] and experimental studies on the local mobility in dendrimer molecules[50,51] indicate the same trend. A strong decrease of segmental diffusion with G value followed by an analogous slow-down of long-time diffusion has been reported in ^{13}C NMR studies in PAMAM dendrimers.[52] In the following sections, the diffusion and the dynamic properties of our models are investigated in order to address these observations.

A. Diffusion behavior

Dependence of the mean square displacement $\langle \Delta r^2(t) \rangle$ (MSD) of a generation's center of mass is shown in Fig. 7. The initial increase of the MSD depends on the molecular weight of the dendrimer (decreases with increasing G). The inset of Fig. 7 illustrates the dependence of the center-of-mass diffusion coefficients on the number of UAs within the dendrimer as extracted by the long-time slopes of the MSD curves. A line of slope -0.5 is shown which was the theoretically predicted behavior for the diffusion of dendrimer models at Θ conditions under the Zimm approximation (see Fig. 8 of Ref. 31 at the high excluded volume limit). In Fig. 8, the diffusion behavior is resolved over the different g shells for the lowest and the highest generation models examined. The effective MSD of a g shell is calculated by averaging over the MSDs of the beads belonging to this shell. The diffusion of the center of mass of the whole dendrimer is shown for comparison as well. At short times, a gradual retardation of the MSD from the outer shell toward the core is observed. Diffusion of the shells belonging to the $G6$ dendrimer exhibit a stronger dependence (i.e., slowing down) on the shell number. This behavior persists to longer time scales compared to the $G3$ case resulting in overall

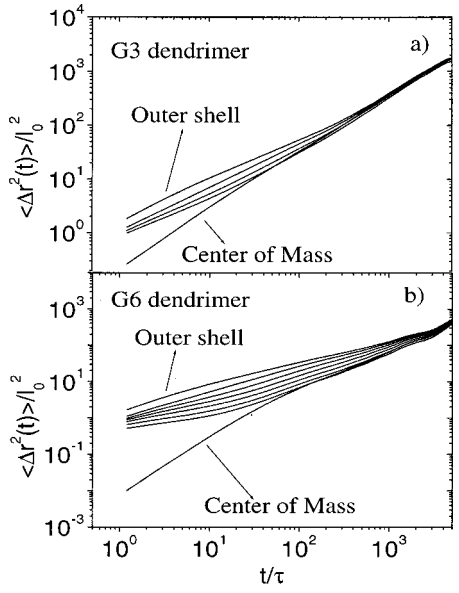

FIG. 8. Mean square displacement resolved in generation shells (a) $G3$ dendrimer, (b) $G6$ dendrimer.

slower diffusion. Such a picture is consistent with the experimentally observed dependence of the local mobility on dendrimer size.

B. Dynamic properties

^{13}C and ^{2}H NMR experiments[52,53] in PAMAM dendrimers revealed a marked dependence (i.e., slowing down) of average segmental relaxation times with molecular weight. Additionally, segmental motion at dendrimer termini was found to be significantly faster compared to the interior sites. Meltzer *et al.*[52,53] interpreted their results in the context of the Lescanec–Muthukumar[44] model, which invokes a density profile with a maximum at the core followed by a monotonic decrease toward the exterior of the molecule. Their reasoning is based on the strong molecular weight dependence of the density profile which might affect the segmental mobility particularly at radial distances close to the core. However, predictions of this model like the shape of the density profile and the scaling of the molecular size are not in accord with later studies[14,18,20,23,25,33] (including the present work), while criticism has been raised concerning the ability of the kinetic growth procedure used to produce equilibrium structures.[20,33,54]

In order to address these observations in detail, the trajectories have been analyzed over a broad range of time and length scales. Local dynamics were studied through the autocorrelation functions' (ACFs) decay of the bonds while longer length-scale motions are investigated by monitoring the relaxational behavior of the *core-to-g-shell* (CTg) vectors. As is schematically illustrated in Fig. 9, the CTg (dotted) vectors connect the topological center with beads belonging to distinct g shells. Therefore, this notation will refer to a vector originating at the core and ending in any of the beads belonging to the gth shell of a dendrimer. Autocorrelation functions $C(t)$ were calculated as $C(t)=\langle \cos\theta(t)\rangle = \langle \hat{\mathbf{v}}(0)\cdot\hat{\mathbf{v}}(t)\rangle$. $\hat{\mathbf{v}}(0)$ and $\hat{\mathbf{v}}(t)$ denote unit vectors in the direction of a vector $\mathbf{v}$ at times 0 and t, respectively. The angular brackets represent an average over the different time origins and an average over all similar CTg vectors.

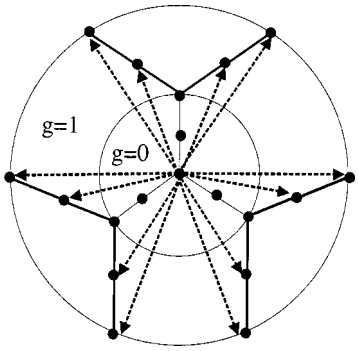

FIG. 9. Schematical illustration of the bond and the core-to-g-shell vectors for $g=1$. Bond vectors belonging to the first generational shell are shown by thick solid lines. CT1 vectors are represented by the dashed lines.

1. Data analysis method

Analysis of the correlation functions is performed in terms of their distribution of relaxation times (DRTs).[55] The need to invoke a distribution of correlation times for a more accurate interpretation of relevant T_1 NMR data has earlier been noticed.[52] In this approach, each $C(t)$ is described as a continuous distribution of exponential processes according to the expression $C(t)=\int_{-\infty}^{\infty} F(\ln(\xi))e^{-t/\xi}d\ln\xi$, where $F(\ln(\xi))$ symbolizes the normalized DRT.[56] Information associated with the existence of distinct motional processes and the dispersion of exponential decays describing each process is extracted from the number and the width of the peaks appearing in the DRTs, respectively. A characteristic time (CT) for the ith process appearing in the spectra (not to be confused with the time unit τ defined in Sec. II B) can be calculated as $\tau_i=\int_{\Delta t_i} tF(\ln(t))d\ln t/\int_{\Delta t_i} F(\ln(t))d\ln t$ where Δt_i denotes the time interval over which the ith peak extends. In case of almost symmetric peaks, the location of the maximum provides a good estimate of the CT. If the integration is performed over the entire time window, an average time τ_{av} is calculated which is equivalent to a time defined as $\tau_{av}=\int_0^{t_{max}} C(t)dt$.

2. Global reorientational motion

As mentioned earlier, dynamics on long length scales are probed by the relaxational behavior of the CTg vectors. The reorientational motion of the entire dendrimer can approximately be represented by the dynamics of these vectors when g refers to the outermost shell. This argument would strictly be true if the outer surface of the molecule were occupied exclusively by beads of the outermost shell. However, it is still a good approximation since beads belonging to the external shell are more probable to be further from the core and thus closer to the surface (see inset of Fig. 4).

Figure 10(a) displays the ACFs of the outermost g shells of the $G3$, $G4$, $G5$, and $G6$ dendrimers. Corresponding DRT spectra are shown in Fig. 10(b). DRTs for $G3$, $G4$, and $G5$ exhibit a double peak. A high amplitude/long time-scale

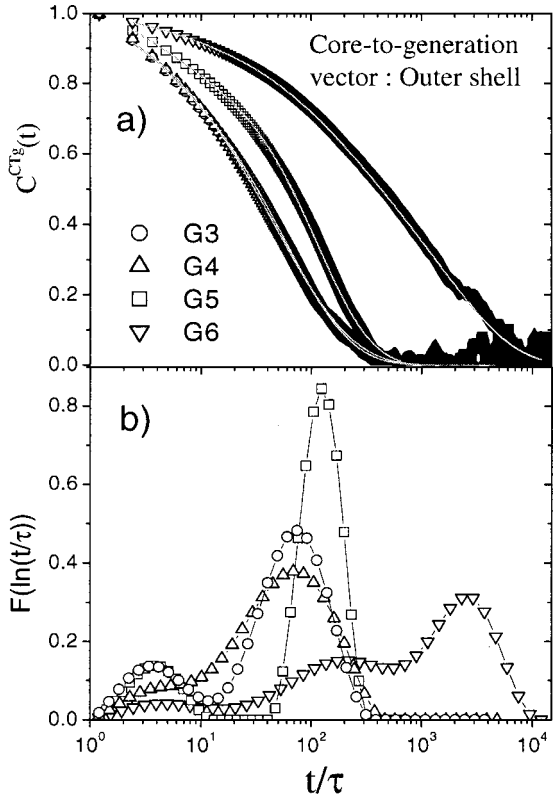

FIG. 10. (a) ACFs for the CTg vectors of the exterior generational shells. Lines through the points represent the fit resulted from application of expression (1). The behavior of the ACFs corresponding to G3 and G4 dendrimers are almost identical. (b) Corresponding DRTs.

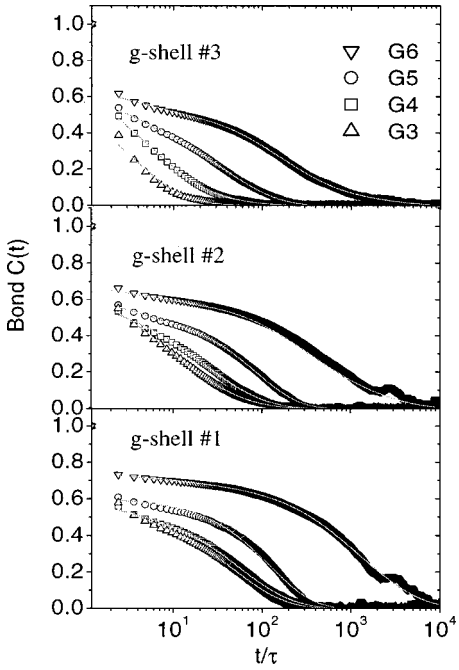

FIG. 11. Comparison of ACFs of bond vectors located in three innermost g shells ($g=1,2,3$). Lines through the points represent the fit resulted from the analysis procedure described by expression (1).

mode is located around 100 ps with a low amplitude/short time mode observed on the time scale of a few ps. The relative amplitude of the fast process is less than 20% in all cases. The slow process apparently reflects the slow reorientation of the dendrimer as a whole, which is the main mechanism for the decorrelation of CTg vectors' ACFs. The low amplitude mode can be attributed to the small contribution expected from bond reorientation. In contrast, the DRT for the $G6$ dendrimer consists of three relaxational processes. The extremely weak fast mode and the intermediate process occur on time scales comparable to the fast and the slow modes of the $G3-G5$ dendrimers. The third relaxation process for $G6$ has the highest amplitude and is more than a decade slower compared to the intermediate mode. This observation suggests that above a characteristic size drastic changes take place on the mechanism through which reorientation of the dendrimer is realized.

3. Local scale dynamics

Figure 11 compares ACFs of bond vectors belonging to inner g shells for all the examined dendrimers. Three *iso-shell* groups of ACFs are depicted: (a) $g=3$, (b) $g=2$, (c) $g=1$ (for the shell numbering convention see Fig. 1). The molecular weight dependence of the spectral characteristics (shape, decay rate) of the ACFs is evident. At a given shell, bond reorientation slows down with dendrimer size. At a given molecular weight, faster decorrelation is observed as g shells draw away from the core. A "relaxation map" of the average correlation times τ_{av} is displayed in Fig. 12. Solid lines connect points corresponding to shells of the same dendrimer (iso-G). Dotted lines connect points of shells of different dendrimers, but at the same distance from each dendrimer's outer shell (equidistant from the "surface," referred to as *iso-D* hereafter). Apart from the dependence of the correlation times on molecular weight (compare times at constant shell number) and on the distance from the core (compare times at different shells of iso-G curves), some additional features are worth noting. For the three lower size models $G3$, $G4$, $G5$, an apparent insensitivity of τ_{av} to shell

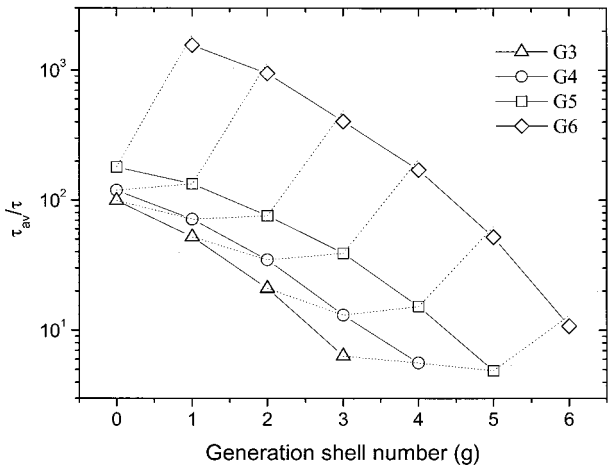

FIG. 12. Average relaxation times for the bond ACFs, resolved in all the generation shells comprising each dedrimer. Solid lines connect points belonging to the same dendrimer. Dotted lines connect points corresponding to shells of different dendrimers, at a constant distance from the outermost shell.

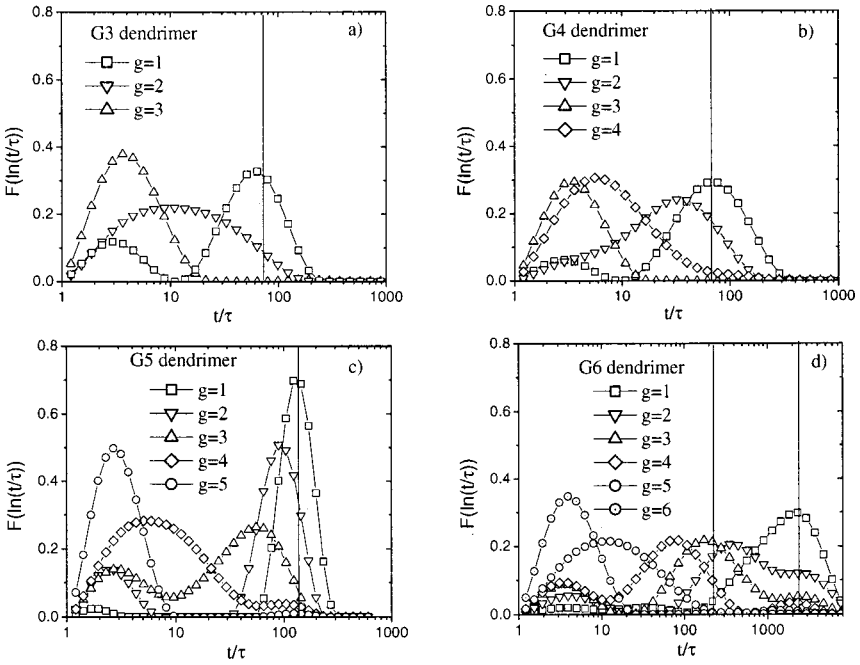

FIG. 13. DRT spectra of the ACFs of the generational shells for the examined dendrimers. The perpendicular lines mark the peak locations of the processes of core-to-g-shell ACF DRT spectra (see the text).

number along the *iso-D* curves is observed. $G6$ can approximately be embodied in the same argument only when considering the outermost shell. The latter notion is consistent with observations from NMR measurements[52] where relaxation times from dendrimer chain termini exhibit the weakest molecular weight dependence compared to internal sites. In general, a significant overall retardation of bond reorientation takes place upon increase of molecular weight between the $G5$ and the $G6$ dendrimer.

Figure 13 shows the DRT spectra corresponding to the ACFs of bonds residing in the different generational shells of each dendrimer. Note that DRTs referring to $g=1,2,3$ describe the corresponding ACFs displayed in Fig. 11. Vertical lines serve in marking the position of the maxima occurring in the DRTs of the corresponding exterior CTg ACFs (excluding that of the fast bond reorientation) presented in Fig. 10(b). Focusing on the smallest size model [Fig. 13(a)], the outer shell's spectra possesses a single peak structure with maxima around 3 ps. The second shell's DRT shows a rather broad peak extending over two decades. The DRT of the-closest-to-the-core shell is bimodal signifying that relaxation occurs on two characteristic time scales. The peak location of the fast process resides at the fast side of the broad second shell's spectra, and practically coincides with that of the outer shell's DRT. The other process being more than a decade slower, overlaps with the long-time tail of the second shell's DRT.

The higher amplitude of the slower mode, whose CT lies on top of that of the dominant slow mode of the CT3 vector (marked by the vertical line), indicates that local relaxation close to the core is mainly attained through overall dendrimer rotation. The fast peak possessing the lower amplitude implies the existence of bond reorientation at time scales of the order of a few ps, in analogy to the fast process appearing in the CT3 DRT. At intermediate distances from the center, a combination of fast and slow dynamics results in a broad distribution extending over the entire dynamic window. At the external shell, fast bond reorientation takes over as the principal motional mechanism.

The degree of coupling between fast and slow time scales of dendrimer motion appears to depend on the size of the dendrimer. Figures 13(b), 13(c), and 13(d) present the analogous DRT spectra corresponding to $G4$, $G5$, and $G6$ dendrimers, respectively. In the $G4$ model, the spectral characteristics of the DRTs for the two endmost shells resemble those of their $G3$ analogs. A notable difference though is that at the innermost shell the relative amplitude of the slow process has been enhanced at the expense of the faster mode (compare the relative peak areas between the slow and the fast processes at innermost shells for $G3$ and $G4$ dendrimers). In other words, the overall dendrimer rotation (represented by the slow process) has an increasing influence on local scale relaxation close to the topological center with increasing molecule size. DRTs of intermediate shells are broader, with ''tails'' instead of the more flattened intermediate spectra in $G3$, through which passage from one extreme time scale to the other takes place. These trends continue in the $G5$ model leading to a stronger separation between the modes. Local relaxation in the shell adjacent to the core is almost ''in phase'' (i.e., relaxes exclusively) with the slow component of the overall dendrimer reorientation. This mode separation persists at higher generational shells ($g=2,3$) as manifested by their bimodal distributions. At even higher molecular weight, the relaxation picture becomes more complex in analogy to the CT6 behavior [Fig. 10(b)]. DRTs of shells 1 and 6 exhibit features similar to the smaller dendrimers' spectra, i.e., they are governed by the two extreme time scales discussed before. At in-between shells local reorientation is instead realized via intermediate time scales.

V. SUMMARY/DISCUSSION

The radius of gyration of the examined models has been found to scale by approximately the third power of molecular weight suggesting three-dimensional compact objects in agreement with recent theoretical, computational, and experimental results obtained for similar models. The calculated form factors approach the structure factor of a sphere as the generation number increases. The same trend is shown from the aspect ratios of the inertia eigenvalues. No abrupt change of the moment of inertia eigenvalues is observed as reported in previous simulations,[15] indicating a rather smooth and continuous transition toward a spherical shape. This transition is accommodated by an increase of the degree of backfolding from virtually all the g shells.

Diffusion at early times and local length scales is found to be molecular-weight dependent in accordance with experiment. Overall diffusion at the long-time limit appears to scale with molecular weight with an exponent close to -0.5 in line with recent theoretical predictions for similar dendrimer models in conditions corresponding to the Θ state of linear chains.

The time scale of local dynamics close to the topological center is essentially determined by the overall dendrimer motion, which in turn depends on the molecular size. On the other hand, molecular weight-independent fast reorientation becomes the principal relaxation mechanism at sites remote from the core and close to the dendrimer periphery. These findings rationalize experimental observations regarding the molecular weight dependence of local relaxation within the interior of a dendrimer and the much faster and virtually molecular weight-independent dynamics of sites furthest from the core. Moreover, at high generations where the average core-to-surface separation is increased, intermediate time scale dynamics characterize local relaxation at generational shells residing in between the two extreme ($g=1$ and $g=G$) shells. This behavior can be visualized as an effective ''*dynamic layering*.'' Local motions within the interior of the dendrimer are bounded by a ''slow layer'' on the time scale of the overall dendrimer motion composed of a few generations close to the core and a ''fast layer'' on the time scale of bond reorientation consisting of beads within the outermost g shell. The interior time scales are expected to depend on the specific topological features of the dendrimers such as the branching functionality and the number of spacer bonds between the branching points. Further understanding and exploitation of ''dynamic layering'' could be of potential use for time-dependent release of host molecules (e.g., in a controlled drug-delivery mechanism).

In conclusion, we have presented a comprehensive molecular dynamics study on static and dynamic properties of molecules of perfect dendritic topology (see Fig. 1) as a function of molecular size, in explicit-solvent solutions. Evaluation of our simulation models by examination of their static characteristics resulted in a close agreement with experimental observations in similar systems. Special emphasis was given in identifying the mechanisms through which orientational relaxation is realized in different length and time scales. Our results can rationalize relevant experimental findings, leading therefore to a better understanding of the dynamics of these molecules.

ACKNOWLEDGMENTS

The authors would like to thank Dr. Alexey V. Lyulin for helpful discussions. Computer time was made available through the 1997 Joint Research Initiative Scheme. One of the authors (K.K.) is grateful to the EPSRC and IRC in Polymer Science and Technology at the University of Leeds for financial support.

[1] R. Service, Science **267**, 458 (1995).
[2] K. Inoue, Prog. Polym. Sci. **25**, 453 (2000).
[3] F. Zeng and S. Zimmerman, Chem. Rev. **97**, 1681 (1997).
[4] D. Zanini and R. Roy, J. Am. Chem. Soc. **119**, 2088 (1997).
[5] F. C. Szoka, Jr. and J. Haensler, U.S. Patent 93-92200, University of California.
[6] Y. Kim and O. Webster, Macromolecules **25**, 5561 (1992).
[7] M. Johansson, E. Malmstrom, and A. Hult, TRIP **4**, 398 (1996).
[8] T. Mourey, S. Turner, M. Rubinstein, J. Frechet, C. Hawker, and K. Wooley, Macromolecules **25**, 2401 (1992).
[9] S. Uppuluri, S. Keinath, D. Tomalia, and P. Dvornic, Macromolecules **31**, 4498 (1998).
[10] M. Hedenqvist, H. Yousefi, E. Malmstrom, M. Johansson, A. Hult, U. Gedde, M. Trollsas, and J. Hedrick, Polymer **41**, 1827 (2000).
[11] A. Lyulin, G. Davies, and D. Adolf, Macromolecules **33**, 3294 (2000).
[12] O. Matthews, A. Shipway, and J. Stoddart, Prog. Polym. Sci. **23**, 1 (1998).
[13] M. Fischer and F. Voegtle, Chem. Rev. **38**, 884 (1999).
[14] S. Stechemesser and W. Eimer, Macromolecules **30**, 2204 (1997).
[15] A. Naylor and W. Goddard, J. Am. Chem. Soc. **111**, 2339 (1989).
[16] B. Hammouda, J. Polym. Sci., Part B: Polym. Phys. **30**, 1387 (1992).
[17] P. Biswas and B. J. Cherayil, J. Chem. Phys. **100**, 3201 (1994).
[18] D. Boris and M. Rubinstein, Macromolecules **29**, 7251 (1996).
[19] W. Carl, J. Chem. Soc., Faraday Trans. **92**, 4151 (1996).
[20] M. Murat and G. S. Grest, Macromolecules **29**, 1278 (1996).
[21] D. A. Tomalia, Macromolecular Symposia **101**, 243 (1996).
[22] A. de Padua, J. A. de Miranda Neto, I. M. Xavier, and F. Moraes, J. Math. Chem. **22**, 97 (1997).
[23] T. J. Prosa, B. J. Bauer, E. J. Amis, D. A. Tomalia, and R. Scherrenberg, J. Polym. Sci., Part B: Polym. Phys. **35**, 2913 (1997).
[24] L. Cavallo and F. Fraternali, Chem.-Eur. J. **4**, 927 (1998).
[25] R. Scherrenberg, B. Coussens, P. vanVliet, G. Edouard, J. Brackman, E. de Brabander, and K. Mortensen, Macromolecules **31**, 456 (1998).
[26] A. Topp, B. J. Bauer, T. J. Prosa, R. Scherrenberg, and E. J. Amis, Macromolecules **32**, 8923 (1999).
[27] C. Gorman and J. Smith, Polymer **41**, 675 (2000).
[28] M. Bhalgat and J. Roberts, Eur. Polym. J. **36**, 647 (2000).
[29] M. Mansfield, Macromolecules **33**, 8043 (2000).
[30] C. Cai and Z. Chen, Macromolecules **30**, 5104 (1997).
[31] Z. Y. Chen and C. Z. Cai, Macromolecules **32**, 5423 (1999).
[32] F. Ganazzoli, Macromolecules **33**, 6611 (2000).
[33] M. Mansfield and L. Klushin, Macromolecules **26**, 4262 (1993).
[34] C. Pierleoni and J.-P. Ryckaert, J. Chem. Phys. **11**, 8539 (1992).
[35] B. Dünweg and K. Kremer, Phys. Rev. Lett. **66**, 2996 (1991).
[36] B. Dünweg and K. Kremer, J. Chem. Phys. **9**, 6983 (1993).
[37] C. Pierleoni, Ph.D thesis, University of Brussels, 1992.
[38] P. Pant, J. Han, G. Smith, and R. Boyd, J. Chem. Phys. **99**, 597 (1993).
[39] A. Rey, J. Freire, and G. de la Tore, Macromolecules **20**, 3304 (1987).
[40] F. Ganazzoli and R. La Ferla, J. Chem. Phys. **113**, 9288 (2000).
[41] T. Forester and W. Smith, CCLRC, Daresbury Laboratory, Daresbury, Warrington Wa4 4AD, England, DL_POLY. DL_POLY is a parallel molecular dynamics package developed at Daresbury laboratory, and is a property of the Council for the Central Laboratory of the Research Councils (CCLRC).
[42] D. Pötschke, M. Ballauff, P. Linder, M. Fischer, and F. Vögtle, Macromolecules **32**, 4079 (1999).
[43] P. de Gennes and H. Hervet, J. Phys. (France) **44**, L351 (1983).
[44] R. Lescanec and M. Muthukumar, Macromolecules **23**, 2280 (1990).
[45] K. Wooley, C. Klug, K. Tasaki, and J. Scaefer, J. Am. Chem. Soc. **119**, 53 (1997).

[46] I. Sendijarevic and A. McHugh, Macromolecules **33**, 590 (2000).
[47] C. Gorman, M. Hger, B. Purkhurst, and J. Smith, Macromolecules **31**, 815 (1998).
[48] M. L. Mansfield and L. I. Klushin, J. Phys. Chem. **96**, 3994 (1992).
[49] A. Ramzi, B. Bauer, R. Scherrenberg, P. Froehling, J. Joosten, and E. Amis, Macromolecules **32**, 4983 (1999).
[50] B. Stark, B. Stühn, H. Frey, C. Lach, K. Lorenz, and B. Frick, Macromolecules **31**, 5415 (1998).
[51] S. Emran, G. Newkome, C. Weis, and J. Harmon, J. Polym. Sci., Part B: Polym. Phys. **37**, 2025 (1999).
[52] A. D. Meltzer, D. A. Tirrell, A. A. Jones, P. T. Inglefield, D. M. Hedstrand, and D. A. Tomalia, Macromolecules **25**, 4541 (1992).
[53] A. D. Meltzer, D. A. Tirrell, A. A. Jones, and P. T. Inglefield, Macromolecules **25**, 4549 (1992).
[54] Z. Chen and C. Cai, Macromolecules **29**, 7943 (1996).
[55] S. Provencher, Comput. Phys. Commun. **27**, 229 (1982).
[56] The DRTs presented henceforth are chosen among almost identical (in terms of the number, the location and the shape of the peaks) solutions for $F(\ln \xi)$, possessing the minimum degree of information (i.e., number of peaks) absolutely necessary to fit the data.